

Real-space Loop Current Pattern in Time-reversal-symmetry Breaking Phase in Kagome Metals

Koki Shimura¹, Rina Tazai², Youichi Yamakawa¹, Seiichiro Onari¹, and Hiroshi Kontani¹

¹*Department of Physics, Nagoya University, Furo-cho, Nagoya 464-8602, Japan*

²*Yukawa Institute for Theoretical Physics, Kyoto University, Kyoto 606-8502, Japan.*

(Dated: February 28, 2024)

The charge loop current (cLC) state has attracted increasing attention in kagome metals. Here, we calculate the currents along the nearest sites i and j , $J_{i,j}$, induced by the cLC order that is the imaginary and odd-parity hopping integral modulation $\delta t_{i,j}$. We reveal that the magnitude of $J_{i,j}$ strongly depends on the nearest sites i and j in the 2×2 cLC state, where $\eta \equiv |\delta t_{i,j}|$ is equivalent for all nearest sites. The obtained $J_{i,j}$ becomes large near the van-Hove singularity (vHS) filling ($n \sim n_{\text{vHS}}$) even when η is fixed. Interestingly, the obtained $J_{i,j}$ exhibits the logarithmic divergence behavior at low temperatures for $n \sim n_{\text{vHS}}$ with a fixed η , by reflecting the vHS points that are the characteristic of kagome metals. The present study provides useful information for local electronic state measurements, such as the site-selective NMR and STM experiments.

Introduction - In recent years, kagome lattice metals have become one of central topics in the field of strongly correlated electron systems. Multiple exotic metallic phase transitions, such as the star-of-David bond-order (BO), superconducting (SC) state, and time-reversal-symmetry-breaking (TRSB) phase without spin polarization, are realized thanks to the strong geometrical frustration that prevents simple spin and charge orders. In AV_3Sb_5 ($A=\text{Cs,Rb,K}$), the 2×2 BO appears at $T_{\text{BO}} \approx 100\text{K}$ [1, 2]. Inside the BO phase, the SC state appears at $T_{\text{SC}} \approx 1 - 10\text{K}$ [3–7]. In addition, the electronic nematic state has been observed inside [8–10] and outside [11] of the BO phase. To explain the observed nematicity, the single- Q odd-parity BO [12] and E_g symmetry nematic BO [13] have been proposed theoretically.

To understand these exotic electronic states in kagome metals, various theoretical studies have been performed, based on the extended mean-field theory [14, 15], the functional renormalization group (RG) theory [16, 17], the parquet RG theory [18, 19], and the density-wave (DW) equation analysis with the higher-order vertex corrections (VCs) [20]. Both the RG theory and the DW equation theory have been successfully applied to Fe-based [21–26] and cuprate superconductors [27]. The nematic order and the BO in these systems originate from the higher-order VCs [24]. Recently, the present authors proposed a unified explanation for the BO and the heavily anisotropic s wave SC state in kagome metals based on the DW equation analysis [20]. This analysis also predicts the emergence of the electronic toroidal quadrupole order in CsTi_3Bi_5 [28]. However, theoretical understanding for the TRSB state has been limited until recently.

Recently, the TRSB state has been observed by various experimental methods. Inside the BO phase, the TRSB has been observed by the STM [1], the μSR [29–31], the anomalous Hall effect [32, 33], and the magnetochiral anisotropy (eMChA) [34, 35] measurements. The spontaneous charge loop-current (cLC) order is a natural candidate of the TRSB order. In kagome metals, the

2×2 cLC order has finite orbital magnetization M_{orb} ; see Ref. [12]. References [34, 35] report that the TRSB domains with random chiralities are detwinned by the magnetic field $h_z \sim 1\text{T}$, and T_{TRSB} is drastically enhanced by small h_z as well as the uniaxial pressure ϵ . Such drastic h_z - and ϵ -dependences of the TRSB states are naturally explained based on the Ginzburg-Landau (GL) theory under (h_z, ϵ) in Ref. [12], owing to the finite M_{orb} . Very interestingly, the TRSB state outside the BO phase ($T_{\text{TRSB}} \approx 130\text{K}$) has been discovered by the recent magnetic torque measurement [11]. The single Q cLC order ($M_{\text{orb}} = 0$) is a natural candidate. Actually, the cLC order can emerge above T_{BO} theoretically [36].

The cLC order was originally studied in cuprate superconductors [37–39]. The cLC order is defined as the imaginary and odd-parity hopping integral modulation between sites i and j , $\delta t_{i,j}$ [20, 36, 40, 45]. The Berry curvature due to $\delta t_{i,j}$ gives rise to the spontaneous current [41]. To understand the microscopic origin of the cLC order in kagome metals, various theoretical studies have been performed, such as the mean-field theory [14, 15], the parquet RG theory [18, 19], and the DW equation analysis [36]. Importantly, the BO fluctuations in kagome metals mediate not only the SC pairing, but also the cLC order that is the TRSB particle-hole pair condensation; see Ref. [36]. Therefore, the cLC state is naturally expected to occur in kagome metals with the BO instability. Recently, the competition between the BO, cLC and the SC states is intensively studied based on the GL theories [12, 19, 42, 43].

In the cLC state in kagome metal model, the uniform orbital magnetization M_{orb} was recently studied in Ref. [12]. However, the nanoscale charge current flowing between the nearest bonds, $J_{i,j}$, has not been performed to our knowledge. The knowledge of $J_{i,j}$ is significant to understand the local magnetization measurements, such as the μSR [29–31] and the NMR [44] measurements.

In this Letter, we analyze the current $J_{i,j}$ in real space in the 2×2 cLC order phase. We reveal that the mag-

nitude of $J_{i,j}$ strongly depends on the nearest sites (i, j) . The obtained $J_{i,j}$ becomes large near the van-Hove singularity (vHS) filling ($n \sim n_{\text{vHS}}$). Interestingly, $J_{i,j}$ exhibits the logarithmic divergence behavior at low temperatures for $n \sim n_{\text{vHS}}$, by reflecting the vHS points that are the characteristic of kagome metals. The present study provides useful information for local electronic state measurements, such as the site-selective NMR and STM experiments.

Model Hamiltonian with $3Q$ cLC Order - First, we present a 3-site kagome lattice model as shown in Fig. 1 (a). The nearest-neighbor hopping integral is set to $t = -0.5[\text{eV}]$ [47]. To avoid perfect nesting, a 3rd-neighbor hopping integral along sides of two triangles is introduced with $t' = -0.02[\text{eV}]$ as shown in Fig. 1 (a). The unit cell contains three sites, labeled A, B, and C. The vectors between nearest-neighboring sites are defined as \mathbf{a}_{AB} , \mathbf{a}_{BC} , and \mathbf{a}_{CA} . Fig. 1 (b) shows the Fermi surface (FS) of the 3-site kagome lattice model and the nesting vectors \mathbf{q}_n ($n = 1, 2, 3$). Three \mathbf{q}_n vectors connect vHS at the M point.

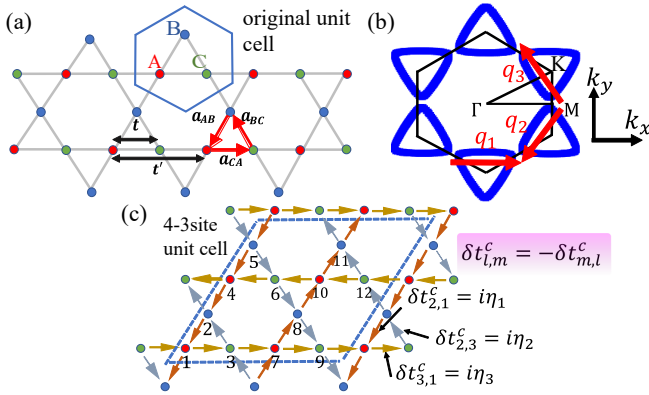


FIG. 1. (Color online) (a) Tight-binding model of the kagome lattice model. (b) FS of the 3-site kagome model at $n = 5.0$. (c) The $3Q$ cLC $\boldsymbol{\eta} = (\eta, \eta, \eta)/\sqrt{3}$ depicted in the kagome lattice.

When the BO or cLC with the nonzero wavevectors \mathbf{q}_n appears in the kagome lattice, the translational symmetry of the system is violated. In the case of a $3Q$ order, the unit cell is extended to include 12 sites. Fig. 1 (c) shows the $3Q$ cLC with the order parameter $\boldsymbol{\eta} = (\eta_1, \eta_2, \eta_3)$, where η_n is current order parameter with \mathbf{q}_n . We assign $\delta t_{i,j}^c = i\eta_1$ [$\delta t_{i,j}^c = -i\eta_1$] for $(l, m) = (1, 2), (2, 4), (4, 5), (5, 1)$ [($l, m) = (7, 8), (8, 10), (10, 11), (11, 7)$], $\delta t_{i,j}^c = i\eta_2$ [$\delta t_{i,j}^c = -i\eta_2$] for $(l, m) = (2, 3), (3, 11), (11, 12), (12, 2)$ [($l, m) = (5, 6), (6, 8), (8, 9), (9, 5)$], and $\delta t_{i,j}^c = i\eta_3$ [$\delta t_{i,j}^c = -i\eta_3$] for $(l, m) = (4, 6), (6, 10), (10, 12), (12, 4)$ [($l, m) = (1, 3), (3, 7), (7, 9), (9, 1)$]. Here, $\delta t_{i,j}^c$ is the purely imaginary ($(\delta t_{i,j}^c)^* = -\delta t_{i,j}^c$) symmetry breaking term of the hopping integral, which is odd parity ($\delta t_{i,j}^c = -\delta t_{j,i}^c$) [36].

The Hamiltonian with the current order is given by

$$\hat{H} = \sum_{\mathbf{k}, l, m} h_{lm}(\mathbf{k}) c_{\mathbf{k}, l}^\dagger c_{\mathbf{k}, m}, \quad (1)$$

l and m indicate the site numbers in the unit cell, with $l, m = 1 \sim 12$. $h_{lm}(\mathbf{k})$ represents the Fourier transformation of $t_{i,j} = t_{i,j}^{(0)} + \delta t_{i,j}^c$, where $t_{i,j}^{(0)}$ is the original hopping integral. An index $i = \{\alpha, l\}$ is employed, where α denotes the unit cell. We introduce the notation $\mathbf{R}_i = \mathbf{R}_\alpha + \mathbf{r}_l$ to designate the position of atoms, where \mathbf{R}_α is the position of the unit cell and \mathbf{r}_l is the relative position of the atom within the unit cell. In the 12-site kagome lattice model, the FS folds, and the M and Γ points in the lattice become equivalent. Therefore, the wave vector of the cLC order is $\mathbf{q}_n = \mathbf{0}$ for $n = 1, 2, 3$ within folded BZ.

Here, we introduce the form factor of the cLC, which is given by the Fourier transformation of $\delta t_{i,j}^c$ shown in Fig. 1 (c). In the 3-site kagome lattice model, the cLC form factor between the nearest site S and site S' ($S, S' = A, B, C$) is given as $f_{SS'}^{\mathbf{q}_n}(\mathbf{k}) = 2 \sin(\mathbf{k} \cdot \mathbf{a}_{SS'})$, where inter-site vector $\mathbf{a}_{SS'}$ and the wavevector \mathbf{q}_n are shown in Fig. 1 (a) and (b), respectively. Here, $n = 1, 2, 3$ for $\{S, S'\} = \{A, B\}, \{B, C\}, \{C, A\}$, respectively. The set of the current order functions is given by $(\eta_1 f_{AB}, \eta_2 f_{BC}, \eta_3 f_{CA})$, where η_n is the n th cLC order parameter. A more detailed explanation is presented in Ref. [20]. Hereafter, we set $\eta_1 = \eta_2 = \eta_3 = \eta$ in the numerical study. We can also present the cLC form factor in the 12-site model, $\tilde{f}_{lm}(k)$, where $l, m = 1 \sim 12$ [12]. For example, $\tilde{f}_{12}(\mathbf{k}) = ie^{-i\mathbf{k} \cdot \mathbf{a}_{12}}$. In this representation, the cLC order wavevector becomes uniform ($\mathbf{q} = \mathbf{0}$), so the incoming and outgoing momenta of $\tilde{f}_{lm}(\mathbf{k})$ are the same. Here, we introduce the 12×12 matrix expression of the current order function $[\hat{C}_{\mathbf{k}}]_{l,m} \equiv \tilde{f}_{lm}(\mathbf{k})$, which is convenient in the present numerical study. Here, $[\hat{C}_{\mathbf{k}}]_{l,m} \neq 0$ only when (l, m) is the pair of the nearest sublattice.

The $3Q$ cLC form factor of kagome metals is derived microscopically from the analysis of the DW equation with the BO fluctuation exchange term as the kernel, as shown in ref. [36]. The $\delta t_{i,j}$ derived in ref. [36] has the same absolute value for all nearest-neighbor bonds (i, j) , meaning $|\delta t_{i,j}^c| = \eta$. It is worth noting that the $\delta t_{i,j}$ derived in ref. [36] also has long-range components, but for simplicity in this paper, we consider only the nearest-neighbor components.

We show the band structure, density of states (DOS), and FS of the 12-site kagome lattice model that cLC order is introduced at $\eta = 0.1$ in Fig 2. In the 12-site model, vHS exists at the M-point, leading to a large DOS. The introduction of cLC order resolves the strong degeneracy near the M point, while the large magnitude of the DOS remains.

Next, to calculate the charge current in the cLC phase, we introduce the current order operator from Heisen-

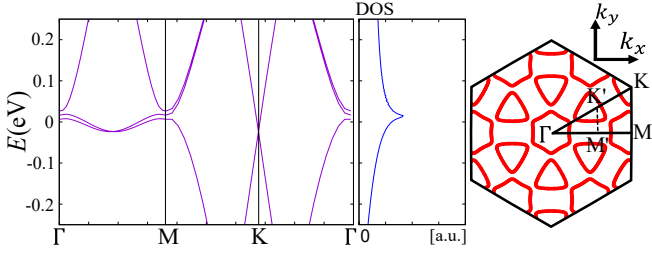


FIG. 2. (Color online) Band structure, DOS, and FS of the 12-site kagome lattice model with $\eta = 0.1$.

berg eq. $\dot{n}_i = -i[n_i, H] = -i(\sum_j t_{i,j} c_i^\dagger c_j - \sum_j t_{j,i} c_j^\dagger c_i)$. Then, the current operator is derived from the continuity equation as

$$j_{i,j} = -i(t_{i,j} c_i^\dagger c_j - (i \leftrightarrow j)). \quad (2)$$

By taking the expectation value with respect to grand canonical ensemble, the current from site j to site i is given as

$$J_{i,j} = \langle j_{i,j} \rangle = it_{i,j} g_{j,i} - (i \leftrightarrow j), \quad (3)$$

where the equal time Green function is given as $g_{i,j} = \lim_{u \rightarrow 0} \langle T c_i^\dagger(u) c_j(0) \rangle$. $\langle \dots \rangle$ represents the mean value for the grand canonical ensemble. The Green function in momentum representation is

$$G_{l,m}(\mathbf{k}, i\epsilon_n) = ((i\epsilon_n + \mu)\hat{1} - \hat{h}(\mathbf{k}))_{l,m}^{-1}. \quad (4)$$

We derive the equal time Green function by the Fourier transform of Eq. (4) as $g_{i,j} = T \sum_{n,\mathbf{k}} G_{l,m}(\mathbf{k}, i\epsilon_n) e^{i\mathbf{k} \cdot (\mathbf{R}_\alpha - \mathbf{R}_\beta)} e^{i\epsilon_n \delta}$. Note that the factor $e^{i\epsilon_n \delta}$ is not necessary for $l \neq m$. $\epsilon_n = (2n - 1)\pi T$ is the fermion Matsubara frequency. Here n is integer.

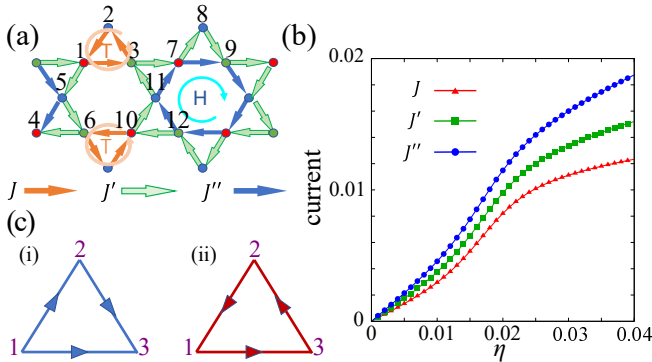


FIG. 3. (Color online) (a) Obtained distribution of the charge currents. Here, $J(J'')$ is the current along the triangular (hexagonal) loop where the direction of each cLC order is aligned. The current on other bonds is given as J' . (b) Obtained currents. (c) 3-site cluster models with different cLC orders. The circulating current in (i) differs from that in (ii); see the text.

Analysis of Current - Now, we present the results of the current distribution induced by the cLC orders. Fig. 3 (a) shows the real-space current distribution within the kagome lattice. The obtained currents as a function of η are shown in Fig. 3 (b) ($T = 2.5\text{meV}$, $n = 5.0$). As η increases, the difference in the magnitude of the currents is enlarged.

To understand the obtained nontrivial relation between $J_{i,j}$ and $\delta t_{i,j}$, here we analyze a simple 3-site cluster model with cLC order oriented in different directions. Fig. 3 (c) represents two 3-site cluster models, (i) and (ii). In the case of (i), δt_{ij}^c is given as $\delta t_{21}^c = \delta t_{31}^c = \delta t_{32}^c = i\eta$. The current $J_{1,2}^1$ that flows in model (i) is derived as $J_{1,2}^1 = -2\eta(t^2 + \eta^2)A$, where $A = T \sum_n [(i\epsilon_n + \mu)^3 + 3(t^2 + \eta^2)(i\epsilon_n + \mu) + 2t(t^2 + \eta^2)]^{-1}$. In the case of (ii), δt_{ij}^c is given as $\delta t_{12}^c = \delta t_{23}^c = \delta t_{31}^c = i\eta$. Then, the current $J_{1,2}^2$ is calculated as $J_{1,2}^2 = 6\eta(t^2 - \frac{\eta^2}{3})B$, where $B = T \sum_n [(i\epsilon_n + \mu)^3 + 3(t^2 + \eta^2)(i\epsilon_n + \mu) + 2t(t^2 - 3\eta^2)]^{-1}$. Thus, different magnitudes of current emerge even when the same order parameter η is provided in three directions $\mathbf{q}_1, \mathbf{q}_2, \mathbf{q}_3$. It holds that $|J_{12}^m| = |J_{23}^m| = |J_{31}^m|$ for each $m = 1, 2$. In the case that $|a| \ll |t|$, $|J_{12}^2| = 3|J_{12}^1|$ holds. In this finite site model, the current converges to zero at $T = 0$ and $T \rightarrow \infty$.

The mathematical reason for the difference in current between (i) and (ii) is that the $J_{1,2}$ given in Eq. (3) includes contributions not only from $\delta t_{1,2}^c$ but also from $\delta t_{2,3}^c$ and $\delta t_{3,1}^c$, which are included in $g_{1,2}$. When the phases of $\delta t_{i,j}^c$ on the closed loop are aligned, i.e., $\delta t_{1,2}^c = \delta t_{2,3}^c = \delta t_{3,1}^c$, the induced current $|J_{i,j}|$ becomes the largest. This consideration leads us to understand why J, J' , and J'' are different in kagome metals as shown in Fig. 3 (a)-(b).

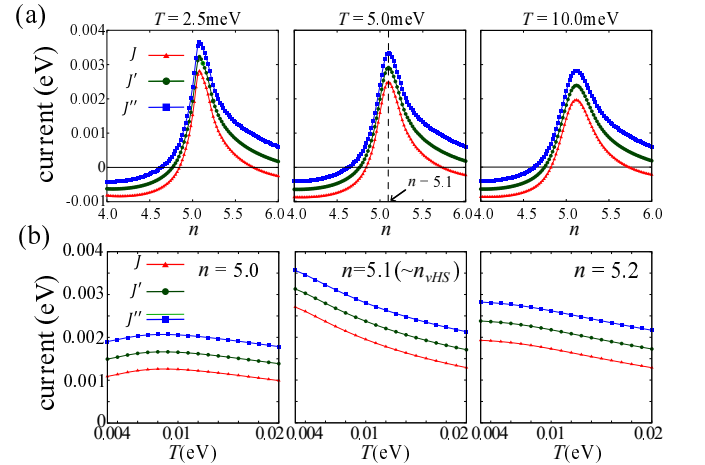


FIG. 4. (Color online) (a) n -dependence of the currents at $T = 2.5 - 10.0\text{meV}$. (b) T -dependence of the currents at $n = 5.0 - 5.2$.

Next, we analyze the filling and temperature depen-

dence of the current. The filling dependence of the current is depicted in Fig. 4 (a). It shows that the current reaches a maximum near the vHS filling. Fig. 4 (b) illustrates the temperature dependence of the current. The magnitude of the current increases at the low-temperatures, with a pronounced increase near the vHS filling.

Susceptibility of the Current - Next stage, we consider susceptibility that describes the behavior of the current. First, we expand the Green function in terms of the order parameter η as $\hat{G}(\mathbf{k}, i\epsilon_n) \sim \hat{G}^{(0)}(\mathbf{k}, i\epsilon_n) + \hat{G}^{(0)}(\mathbf{k}, i\epsilon_n)\eta\hat{C}_\mathbf{k}\hat{G}^{(0)}(\mathbf{k}, i\epsilon_n)$, where $\hat{G}^{(0)}(\mathbf{k}, i\epsilon_n)$ is the Green function with $\eta = 0$. The contribution from the term $\hat{G}^{(0)}(\mathbf{k}, i\epsilon_n)\eta\hat{C}_\mathbf{k}\hat{G}^{(0)}(\mathbf{k}, i\epsilon_n)$ to the current is dominant. The diagrammatic representations of this term is shown in Fig. 5 (a). Meanwhile, the static irreducible susceptibility is

$$\begin{aligned} & \chi_{lm'l'm'}^{J-\eta}(\mathbf{q}) \\ &= -\frac{T}{N} \sum_{\mathbf{k}, n} G_{ll'}^{(0)}(\mathbf{k} + \mathbf{q}, i\epsilon_n) G_{m'm}^{(0)}(\mathbf{k}, i\epsilon_n). \end{aligned} \quad (5)$$

As an example of form factor, $[\hat{C}_\mathbf{k}]_{12} = ie^{i\mathbf{k}\cdot\mathbf{a}_{AB}}$, and $[\hat{C}_\mathbf{k}]_{21} = -ie^{i\mathbf{k}\cdot\mathbf{a}_{BA}}$. Thus, at $\mathbf{k} = 0$ which corresponds to Γ point, $[\hat{C}_0]_{12} = i$ holds. Here, we recall that sites 1,4,7, and 10 belong to the A site, while sites 2,5,8, and 11 belong to B site. In the case of the 12-site kagome lattice model, the form factor exhibits the largest value at the Γ point. Therefore, after approximating it as $[\hat{C}_\mathbf{k}]_{lm} \sim [\hat{C}_0]_{lm}$, $J_{1,2}$ is given as

$$\begin{aligned} J_{1,2} &\propto T \sum_{n, l', m', \mathbf{k}} [G^{(0)}]^{1, l'} \eta [\hat{C}_\mathbf{k}]_{l'm'} [G^{(0)}]^{m', 2} e^{i\mathbf{k}\cdot(\mathbf{R}_\alpha - \mathbf{R}_\beta)} \\ &\sim \sum_{l', m'=1-12} \chi_{12, l'm'}^{J-\eta}(\mathbf{0}) [\hat{C}_0]_{l'm'} \eta. \end{aligned} \quad (6)$$

Importantly, $\chi_{12, l'm'}^{J-\eta}(\mathbf{0})$ becomes large when $\{l', m'\} = \{1, 2\}, \{4, 5\}, \{7, 8\}, \{10, 11\}$, by reflecting the sublattice interference of the pure-type FS [20]. When we focus on the contribution from $\{l', m'\} = \{1, 2\}, \{2, 1\}$, $J_{1,2}$ in Eq. (6) is proportional to $\chi_{12,12}^{J-\eta} - \chi_{12,21}^{J-\eta}$ due to the odd-parity form factor.

Figure 5 (b) shows diagrammatic representations of $\chi_{12, l'm'}^{J-\eta} - \chi_{12, m'l'}^{J-\eta}$. Taking account of the form factors depicted in Fig. 1 (c), the summation of contributions from $\{l, m\} = \{1, 2\}, \{4, 5\}, \{7, 8\}$, and $\{10, 11\}$ leads to $\phi_{12}^{J-\eta} = [\chi_{12,12}^{J-\eta} - \chi_{12,21}^{J-\eta} + \chi_{12,42}^{J-\eta} - \chi_{12,24}^{J-\eta} + \chi_{12,45}^{J-\eta} - \chi_{12,54}^{J-\eta} + \chi_{12,14}^{J-\eta} - \chi_{12,41}^{J-\eta}] - [\chi_{12,78}^{J-\eta} - \chi_{12,87}^{J-\eta} + \chi_{12,10}^{J-\eta} - \chi_{12,8}^{J-\eta} + \chi_{12,10}^{J-\eta} - \chi_{12,11}^{J-\eta} + \chi_{12,7}^{J-\eta} - \chi_{12,10}^{J-\eta} - \chi_{12,10}^{J-\eta} - \chi_{12,7}^{J-\eta}]$.

The filling and temperature dependences of $\phi_{12}^{J-\eta}$ are shown respectively in Fig. 5 (c) and (d). $\phi_{12}^{J-\eta}$ reaches its maximum value at the vHS filling $n_{\text{vHS}} \sim 5.1$, with a notable increase in the low temperature regime. Analytically, at vHS filling, $\phi_{12}^{J-\eta} \propto 1/E_0 (\ln E_0/T)^2 + \chi_{0c}$ when

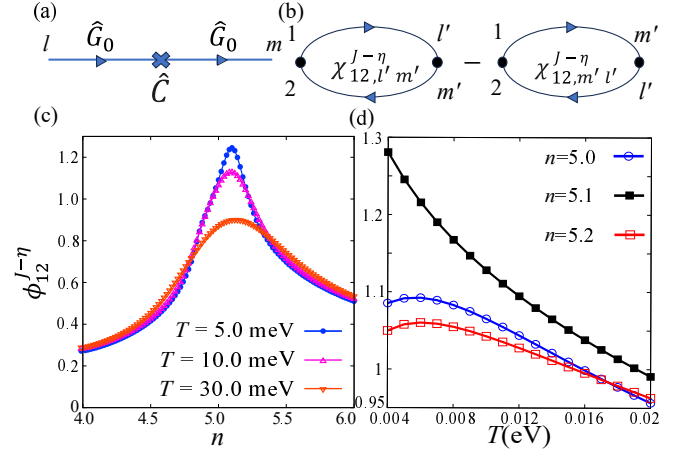


FIG. 5. (Color online) (a) Diagrammatic representation of the first-order term $(\hat{G}^{(0)}\eta\hat{C}\hat{G}^{(0)})_{m,l}$. (b) Diagrammatic representation of the sum of susceptibility $\chi_{12, l'm'}^{J-\eta} - \chi_{12, m'l'}^{J-\eta}$. (c) n -dependence of $\phi_{12}^{J-\eta}$ at $T = 5.0, 10, 30$ meV. (d) Temperature dependence of $\phi_{12}^{J-\eta}$ at $n = 5.0 - 5.2$

$E_0 \sim 0.1$ [eV] is the energy range where the vHS band-structure is well described by the quadratic expression, as discussed in Ref. [19]. Here, χ_{0c} is the constraint susceptibility, which excludes the contribution for $|E| < E_0$ from Eq. (5), which is defined in SM in Ref. [46]. This temperature dependence is attributed to the vHS in the kagome lattice model, in stark contrast to usual metals, where $\phi_{12}^{J-\eta}$ remains constant.

The susceptibility $\phi_{12}^{J-\eta}$ can be obtained experimentally by observing η and J_{ij} , which in principle may be derived from the local DOS and the local magnetic-field measurements, respectively. This is an interesting future challenge.

Effect of Self-energy - In addition, we analyze how the current is modified by the self-energy. Fig. 6 (a) shows the filling dependence of the current in the presence of self-energy. Fig. 6 (b) shows the obtained damping rate γ dependence of current. As γ increases, the current is gradually suppressed.

Summary and Discussions - In this letter, we employed the Green function method to calculate the real-space current distribution in the $3Q$ cLC phase of kagome metal. The obtained magnitude of $J_{i,j}$ strongly depends on the nearest sites (i, j) even when $|\delta t_{i,j}|$ is constant for any bonds. The obtained $J_{i,j}$ becomes large near the vHS filling, while it is suppressed when considering the self-energy. Interestingly, $J_{i,j}$ exhibits the logarithmic divergence behavior at low temperatures for $n \sim n_{\text{vHS}}$. The present study provides useful information for local electronic state measurements, such as the site-selective NMR and STM experiments.

We have employed the Green function method to calculate $J_{i,j}$. Based on this method, one can calculate the

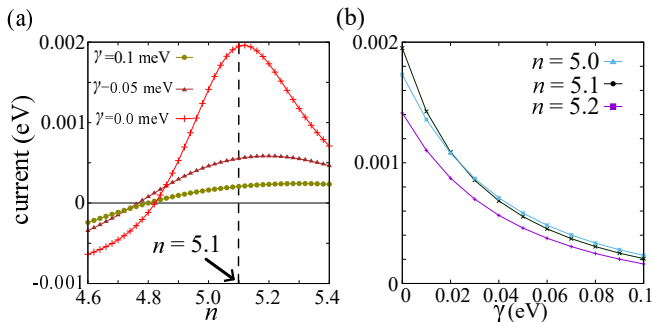


FIG. 6. (Color online) (a) Filling dependence of the current $J^{\min} = \min J, J', J''$ for various γ . (b) γ dependence of J^{\min} for $n = 5.0 - 5.2$.

current by including the beyond-mean-field electron correlations, such as the self-energy and the VCs. This is a great advantage of the present method.

This study has been supported by Grants-in-Aid for Scientific Research from MEXT of Japan (JP20K03858, JP20K22328, JP22K14003, JP23K03299), and by the Quantum Liquid Crystal No. JP19H05825 KAKENHI on Innovative Areas from JSPS of Japan.

- [1] Yu-Xiao Jiang, Jia-Xin Yin, M. Michael Denner, Nana Shumiya, Brenden R. Ortiz, Gang Xu, Zurab Guguchia, Junyi He, Md Shafayat Hossain, Xiaoxiong Liu, Jacob Ruff, Linus Kautzsch, Songtian S. Zhang, Guoqing Chang, Ilya Belopolski, Qi Zhang, Tyler A. Cochran, Daniel Multer, Maksim Litskevich, Zi-Jia Cheng, Xian P. Yang, Ziqiang Wang, Ronny Thomale, Titus Neupert, Stephen D. Wilson, Zahid Hasan *Unconventional chiral charge order in kagome superconductor KV_3Sb_5* , Nat. Mat. **20**, 1353-1357 (2021).
- [2] Hong Li, He Zhao, Brenden R. Ortiz, Takamori Park, Mengxing Ye, Leon Balents, Ziqiang Wang, Stephen D. Wilson, Ilija Zeljkovic *Rotational symmetry breaking in the normal state of a kagome superconductor KV_3Sb_5* , Nat. Phys. **18**, 265 (2022)
- [3] B. R. Ortiz, L. C. Gomes, J. R. Morey, M. Winiarski, M. Bordelon, J. S. Mangum, I. W. H. Oswald, J. A. Rodriguez-Rivera, J. R. Neilson, S. D. Wilson, E. Ertekin, T. M. McQueen, and E. S. Toberer, *New kagome prototype materials: discovery of KV_3Sb_5 , RbV_3Sb_5 , and CsV_3Sb_5* , Phys. Rev. Materials **3**, 094407 (2019).
- [4] B. R. Ortiz, S. M. L. Teicher, Y. Hu, J. L. Zuo, P. M. Sarte, E. C. Schueller, A. M. M. Abeykoon, M. J. Krogstad, S. Rosenkranz, R. Osborn, R. Seshadri, L. Balents, J. He, and S. D. Wilson, *CsV_3Sb_5 : A Z_2 Topological Kagome Metal with a Superconducting Ground State*, Phys. Rev. Lett. **125**, 247002 (2020).
- [5] F. H. Yu, D. H. Ma, W. Z. Zhuo, S. Q. Liu, X. K. Wen, B. Lei, J. J. Ying, and X. H. Chen, *Unusual competition of superconductivity and charge-density-wave state in a compressed topological kagome metal*, Nat. Commun. **12**, 3645 (2021).
- [6] K. Y. Chen, N. N. Wang, Q. W. Yin, Y. H. Gu, K. Jiang, Z. J. Tu, C. S. Gong, Y. Uwatoko, J. P. Sun, H. C. Lei, J. P. Hu, and J.-G. Cheng, *Double Superconducting Dome and Triple Enhancement of T_c in the Kagome Superconductor CsV_3Sb_5 under High Pressure*, Phys. Rev. Lett. **126**, 247001 (2021).
- [7] B. R. Ortiz, P. M. Sarte, E. M. Kenney, M. J. Graf, S. M. L. Teicher, R. Seshadri, and S. D. Wilson, *Superconductivity in the Z_2 kagome metal KV_3Sb_5* , Phys. Rev. Materials **5**, 034801 (2021).
- [8] L. Nie, K. Sun, W. Ma, D. Song, L. Zheng, Z. Liang, P. Wu, F. Yu, J. Li, M. Shan, D. Zhao, S. Li, B. Kang, Z. Wu, Y. Zhou, K. Liu, Z. Xiang, J. Ying, Z. Wang, T. Wu, and X. Chen, *Charge-density-wave-driven electronic nematicity in a kagome superconductor*, Nature **604**, 59 (2022).
- [9] Y. Xu, Z. Ni, Y. Liu, B. R. Ortiz, S. D. Wilson, B. Yan, L. Balents, and L. Wu, *Universal three-state nematicity and magneto-optical Kerr effect in the charge density waves in AV_3Sb_5 ($A=Cs, Rb, K$)*, arXiv:2204.10116.
- [10] H. Li, H. Zhao, B. R. Ortiz, T. Park, M. Ye, L. Balents, Z. Wang, S. D. Wilson, and I. Zeljkovic, *Rotation symmetry breaking in the normal state of a kagome superconductor KV_3Sb_5* , Nat. Phys. **18**, 265 (2022).
- [11] T. Asaba, A. Onishi, Y. Kageyama, T. Kiyosue, K. Ohtsuka, S. Suetsugu, Y. Kohsaka, T. Gaggli, Y. Kasahara, H. Murayama, K. Hashimoto, R. Tazai, H. Kontani, B. R. Ortiz, S. D. Wilson, Q. Li, H. -H. Wen, T. Shibauchi, Y. Matsuda, *Evidence for an odd-parity nematic phase above the charge density wave transition in kagome metal CsV_3Sb_5* , accepted for publication in Nat. Phys. (arXiv:2309.16985).
- [12] Rina Tazai, Youichi Yamakawa, Hiroshi Kontani, *Drastic magnetic-field-induced chiral current order and emergent current-bond-field interplay in kagome metals*, Proc. Natl. Acad. Sci. USA. **121**, e2303476121 (2024).
- [13] Jianxin Huang, Rina Tazai, Youichi Yamakawa, Seichiro Onari, Hiroshi Kontani, *Low temperature phase transitions under CDW state in kagome metals AV_3Sb_5 ($A=Cs, Rb, K$): Significance of mix-type Fermi surface electron correlations*, arXiv:2305.18087.
- [14] M. M. Denner, R. Thomale, and T. Neupert, *Analysis of Charge Order in the Kagome Metal AV_3Sb_5 ($A = K, Rb, Cs$)*, Phys. Rev. Lett. **127**, 217601 (2021).
- [15] Y.-P. Lin and R. M. Nandkishore, *Complex charge density waves at Van Hove singularity on hexagonal lattices: Haldane-model phase diagram and potential realization in the kagome metals AV_3Sb_5 ($A = K, Rb, Cs$)*, Phys. Rev. B **104**, 045122 (2021).
- [16] M. L. Kiesel, C. Platt, and R. Thomale, *Unconventional Fermi Surface Instabilities in the Kagome Hubbard Model*, Phys. Rev. Lett. **110**, 126405 (2013).
- [17] W.-S. Wang, Z.-Z. Li, Y.-Y. Xiang, and Q.-H. Wang, *Competing electronic orders on kagome lattices at van Hove filling*, Phys. Rev. B **87**, 115135 (2013).
- [18] H. D. Scammell, J. Ingham, T. Li, and O. P. Sushkov, *Chiral excitonic order from twofold van Hove singularities in kagome metals*, Nat. Commun. **14**, 605 (2023)
- [19] T. Park, M. Ye, and L. Balents, *Electronic instabilities of kagome metals: Saddle points and Landau theory*, Phys. Rev. B **104**, 035142 (2021).
- [20] R. Tazai, Y. Yamakawa, S. Onari, and H. Kontani, *Mechanism of exotic density-wave and beyond-Migdal unconventional superconductivity in kagome metal AV_3Sb_5 ($A = K, Rb, Cs$)*, Sci. Adv. **8**, eabl4108 (2022).

- [21] S. Onari, Y. Yamakawa, and H. Kontani, *Phys. Rev. Lett.* **112**, 187001 (2014).
- [22] S. Onari, Y. Yamakawa, and H. Kontani, *Phys. Rev. Lett.* **116**, 227001 (2016).
- [23] Y. Yamakawa, S. Onari and H. Kontani, *Phys. Rev. X* **6**, 021032 (2016).
- [24] H. Kontani, R. Tazai, Y. Yamakawa, and S. Onari, *Unconventional density waves and superconductivities in Fe-based superconductors and other strongly correlated electron systems*, *Adv. Phys.* **70**, 355 (2021).
- [25] R. Tazai, S. Matsubara, Y. Yamakawa, S. Onari, and H. Kontani, *Rigorous formalism for unconventional symmetry breaking in Fermi liquid theory and its application to nematicity in FeSe*, *Phys. Rev. B* **107**, 035137 (2023).
- [26] A. V. Chubukov, M. Khodas, and R. M. Fernandes, *Phys. Rev. X* **6**, 041045 (2016).
- [27] M. Tsuchiizu, K. Kawaguchi, Y. Yamakawa, and H. Kontani, *Phys. Rev. B* **97**, 165131 (2018).
- [28] J. Huang, Y. Yamakawa, R. Tazai, and H. Kontani, *Odd-parity intra-unit-cell bond-order and induced nematicity in kagome metal $CsTi_3Bi_5$ driven by quantum interference mechanism*, arXiv:2305.18093.
- [29] C. Mielke, D. Das, J.-X. Yin, H. Liu, R. Gupta, Y.-X. Jiang, M. Medarde, X. Wu, H. C. Lei, J. Chang, P. Dai, Q. Si, H. Miao, R. Thomale, T. Neupert, Y. Shi, R. Khasanov, M. Z. Hasan, H. Luetkens, and Z. Guguchia, *Time-reversal symmetry-breaking charge order in a kagome superconductor*, *Nature* **602**, 245 (2022).
- [30] R. Khasanov, D. Das, R. Gupta, C. Mielke, M. Elender, Q. Yin, Z. Tu, C. Gong, H. Lei, E. T. Ritz, R. M. Fernandes, T. Biro, Z. Guguchia, and H. Luetkens, *Time-reversal symmetry broken by charge order in CsV_3Sb_5* , *Phys. Rev. Research* **4**, 023244 (2022).
- [31] Z. Guguchia, C. Mielke, D. Das, R. Gupta, J.-X. Yin, H. Liu, Q. Yin, M. H. Christensen, Z. Tu, C. Gong, N. Shumiya, M. S. Hossain, T. Gamsakhurdashvili, M. Elender, P. Dai, A. Amato, Y. Shi, H. C. Lei, R. M. Fernandes, M. Z. Hasan, H. Luetkens, and R. Khasanov, *Tunable unconventional kagome superconductivity in charge ordered RbV_3Sb_5 and KV_3Sb_5* , *Nat. Commun.* **14**, 153 (2023).
- [32] S.-Y. Yang, Y. Wang, B. R. Ortiz, D. Liu, J. Gayles, E. Derunova, R. Gonzalez-Hernandez, L. Šmejkal, Y. Chen, S. S. P. Parkin, S. D. Wilson, E. S. Toberer, T. McQueen, and M. N. Ali, *Giant, unconventional anomalous Hall effect in the metallic frustrated magnet candidate, KV_3Sb_5* , *Sci. Adv.* **6**, eabb6003 (2020).
- [33] F. H. Yu, T. Wu, Z. Y. Wang, B. Lei, W. Z. Zhuo, J. J. Ying, and X. H. Chen, *Concurrence of anomalous Hall effect and charge density wave in a superconducting topological kagome metal*, *Phys. Rev. B* **104**, L041103 (2021).
- [34] C. Guo, C. Putzke, S. Konyzheva, X. Huang, M. Gutierrez-Amigo, I. Errea, D. Chen, M. G. Vergniory, C. Felser, M. H. Fischer, T. Neupert, and P. J. W. Moll, *Switchable chiral transport in charge-ordered Kagome metal CsV_3Sb_5* , *Nature* **611**, 461 (2022).
- [35] C. Guo, G. Wagner, C. Putzke, D. Chen, K. Wang, L. Zhang, M. G. Amigo, I. Errea, M. G. Vergniory, C. Felser, M. H. Fischer, T. Neupert, and P. J. W. Moll, *Correlated order at the tipping point in the kagome metal CsV_3Sb_5* , arXiv:2304.00972.
- [36] R. Tazai, Y. Yamakawa, and H. Kontani, *Charge-loop current order and Z_3 nematicity mediated by bond-order fluctuations in kagome metals*, *Nat. Commun.* **14**, 7845 (2023).
- [37] I. Affleck and J. B. Marston, *Large- n limit of the Heisenberg-Hubbard model: Implications for high- T_c superconductors*, *Phys. Rev. B* **37**, 3774(R) (1988).
- [38] C. M. Varma, *Theory of the pseudogap state of the cuprates*, *Phys. Rev. B* **73**, 155113 (2006).
- [39] W. H. P. Nielsen, W. A. Atkinson, and B. M. Andersen, *Signatures of orbital loop currents in the spatially resolved local density of states*, *Phys. Rev. B* **86**, 054510 (2012).
- [40] H. Kontani, Y. Yamakawa, R. Tazai, and S. Onari, *Odd-parity spin-loop-current order mediated by transverse spin fluctuations in cuprates and related electron systems*, *Phys. Rev. Research* **3**, 013127 (2021).
- [41] F. D. M. Haldane, *Model for a Quantum Hall Effect without Landau Levels: Condensed-Matter Realization of the "Parity Anomaly"*, *Phys. Rev. Lett.* **61**, 2015 (1988).
- [42] F. Grandi, A. Consiglio, M. A. Sentef, R. Thomale, and D. M. Kennes, *Theory of nematic charge orders in kagome metals*, *Phys. Rev. B* **107**, 155131 (2023).
- [43] M. H. Christensen, T. Biro, B. M. Andersen, and R. M. Fernandes, *Loop currents in AV_3Sb_5 kagome metals: Multipolar and toroidal magnetic orders*, *Phys. Rev. B* **106**, 144504 (2022).
- [44] J. Luo, Z. Zhao, Y. Z. Zhou, J. Yang, A. F. Fang, H. T. Yang, H. J. Gao, R. Zhou, and G.-q. Zheng, *Possible star-of-David pattern charge density wave with additional modulation in the kagome superconductor CsV_3Sb_5* , *npj Quantum Materials* **7**, 30 (2022).
- [45] R. Tazai, Y. Yamakawa, and H. Kontani, *Emergence of charge loop current in the geometrically frustrated Hubbard model: A functional renormalization group study*, *Phys. Rev. B* **103**, L161112 (2021).
- [46] M. Tsuchiizu, Yusuke Ohno, Seiichiro Onari, and H. Kontani *Orbital Nematic Instability in the Two-Orbital Hubbard Model: Renormalization-Group + Constrained RPA Analysis*, *Phys. Rev. B* **93**, 155148.
- [47] X. Wu, T. Schwemmer, T. Müller, A. Consiglio, G. Sangiovanni, D. Di Sante, Y. Iqbal, W. Hanke, A. P. Schnyder, M. M. Denner, M. H. Fischer, T. Neupert, and R. Thomale, *Nature of Unconventional Pairing in the Kagome Superconductors AV_3Sb_5 ($A = K, Rb, Cs$)*, *Phys. Rev. Lett.* **127**, 177001 (2021).